Cell, Vol. 99, 355–366, November 12, 1999, Copyright ©1999 by Cell Press

A Novel Class of Eukaryotic Zinc-Binding Proteins Is Required for Disease Resistance Signaling in Barley and Development in *C. elegans*

Ken Shirasu,*‖ Thomas Lahaye,*‖# Man-Wah Tan,†‡ Fasong Zhou,* Cristina Azevedo,* and Paul Schulze-Lefert*§

*The Sainsbury Laboratory
John Innes Centre
Colney Lane
NR4 7UH Norwich
United Kingdom

†Department of Molecular Biology
Massachusetts General Hospital
Boston, Massachusetts 02114

‡Department of Genetics
Harvard Medical School
Boston, Massachusetts 02115

Summary

Barley *Rar1* is a convergence point in the signaling of resistance to powdery mildew, triggered by multiple race-specific resistance (*R*) genes. *Rar1* is shown to function upstream of H_2O_2 accumulation in attacked host cells, which precedes localized host cell death. We isolated *Rar1* by map-based cloning. The sequence of the deduced 25.5 kDa protein reveals two copies of a 60–amino acid domain, CHORD, conserved in tandem organization in protozoa, plants, and metazoa. CHORD defines a novel eukaryotic Zn^{2+}-binding domain. Silencing of the *C. elegans* CHORD-containing gene, *chp*, results in semisterility and embryo lethality, suggesting an essential function of the wild-type gene in nematode development. Our findings indicate that plant *R* genes have recruited a fundamental cellular control element for signaling of disease resistance and cell death.

Introduction

Similar to mammals, plants have the capacity to recognize potential pathogens and to mount an efficient defense response (Baker et al., 1997). Recognition of pathogens by plants is mediated by race-specific resistance (*R*) genes. The major class of *R* genes contains a nucleotide-binding site (NBS) and C-terminal leucine-rich repeats (LRR) of various lengths, the NBS-LRRs. A second class comprises genes containing a kinase and/or a LRR domain (Jones and Jones, 1997). Experimental and indirect evidence suggest that the highly variable LRRs in both classes of *R* genes have a major role in recognition of pathogen determinants encoded by cognate genes (*Avr*) in the pathogen (Parniske et al., 1997).

§To whom correspondence should be addressed (e-mail: schlef@bbsrc.ac.uk).
‖These authors contributed equally to this work.
#Present address: Institute of Genetics, Martin-Luther University, Weinbergstrasse 22, D-06120 Halle, Germany.

Although many *R* genes have been cloned and significant advances have been made recently in understanding the interactions between the *R* and *Avr* genes, the molecular basis of signaling immediately following pathogen perception is still largely unknown. The first genetic evidence for additional plant components required in race-specific resistance was obtained from barley mutants and their interaction with the powdery mildew fungus, *Erysiphe graminis* f sp *hordei* (Torp and Jørgensen, 1986). These studies identified two genes, *Rar1* and *Rar2*, which are required for resistance mediated by the *R* gene *Mla-12* (Jørgensen, 1988; Freialdenhoven et al., 1994). Later studies showed that several, but not all, *R* genes against powdery mildew require *Rar1* for their function (Jørgensen, 1996; Peterhänsel et al., 1997).

R gene–mediated resistance is in most cases associated with the activation of a host cell death reaction, the hypersensitive response (HR). HR is generally restricted to sites of attempted infection. Spontaneous cell death mutants have been isolated and characterized from *Arabidopsis* (Dietrich et al., 1994; Greenberg et al., 1994). These mutants exhibit constitutive defense responses even in the absence of pathogens, suggesting that the HR has features of a programmed cell death (PCD). Although there is no experimental evidence for common functional components in PCD of plants and animals, it has been noted that proteins encoded by the NBS-LRR class of plant *R* genes, the *ced-4* gene of *C. elegans* and its human homolog, *APAF1*, share a number of sequence motifs (Van der Biezen and Jones, 1998). In both plants and animals, PCD in response to pathogens appears to be just one out of many physiological mechanisms of cell death (Pennell and Lamb, 1997; Vaux and Korsmeyer, 1999).

A plethora of biochemical changes coincide with *R* gene–triggered resistance and host cell death (Lamb and Dixon, 1997). There is ample evidence for the rapid induction of reactive oxygen intermediates (ROI) such as H_2O_2 and O_2^- following pathogen challenge. Similar to human macrophages or neutrophils, ROI are believed to function in plant defense by either directly killing the pathogen, or indirectly by triggering PCD (Levine et al., 1994). Homologs of gp91, a component of the H_2O_2-generating complex in mammalian neutrophils, have been recently identified in plants (Groom et al., 1996), but their functional role in the HR remains to be proven. To date, no systematic studies have been reported that utilize genetically defined signaling mutants of *R* gene–triggered resistance to test current hypotheses on ROI function.

Here, we show that susceptible *rar1* mutants are impaired in a biphasic H_2O_2 accumulation and localized cell death upon powdery mildew attack, suggesting a signaling function for *Rar1* early in the resistance pathway. Barley *Rar1* has been isolated by map-based cloning. It encodes a novel protein containing two 60–amino acid (aa) *c*ysteine- and *h*istidine-*r*ich *d*omains, designated CHORD. Biochemical analysis of Rar1 protein reveals that CHORD is an autonomous Zn^{2+}-binding domain. Interestingly, homologs of Rar1 are also present in the genomes of all eukaryotes tested, except yeast,

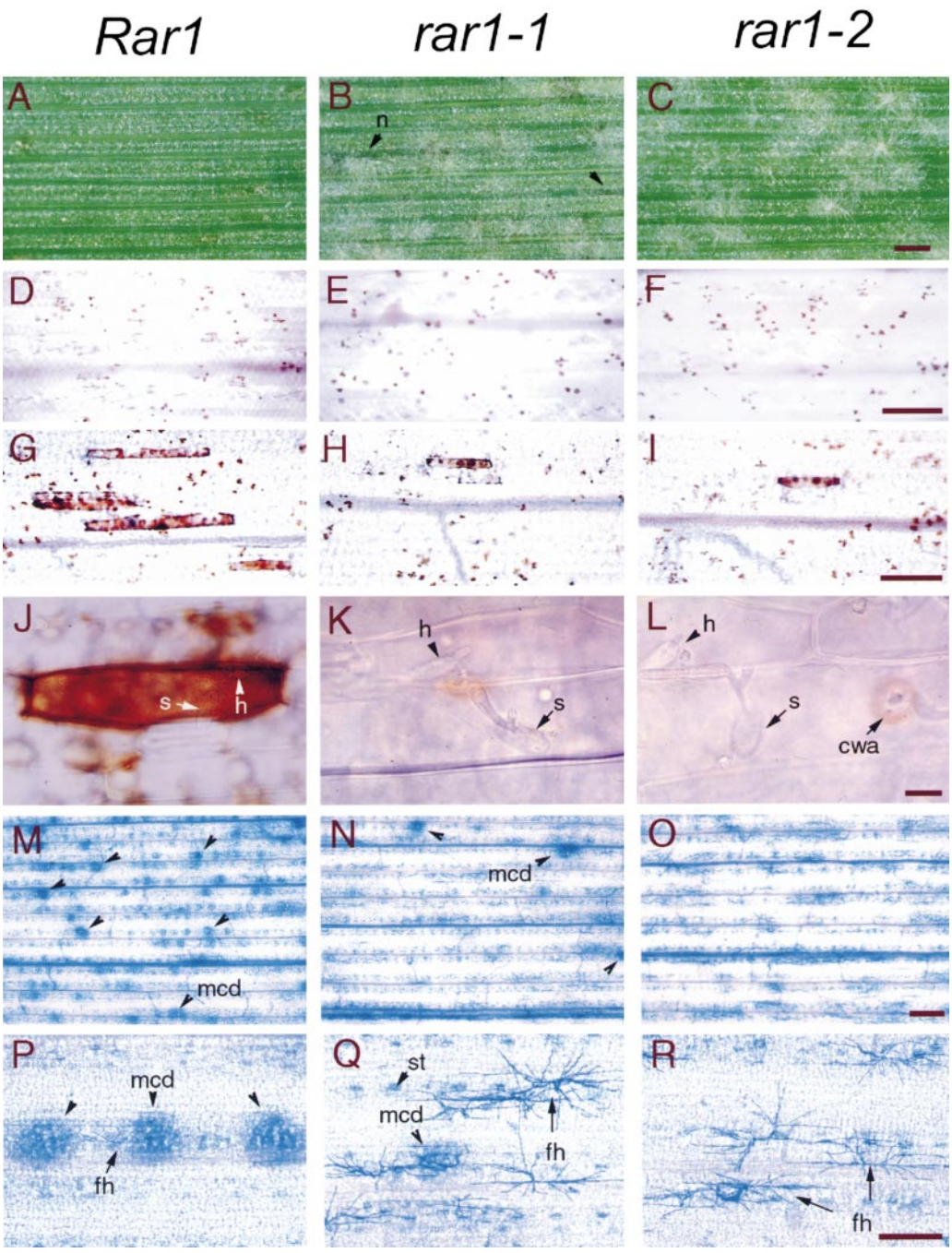

Figure 1. Mutant *rar1* Alleles Compromise Whole-Cell H_2O_2 Accumulation and Cell Death Progression

(A–C) Macroscopic phenotypes of wild-type *Rar1* and mutants *rar1-1* and *rar1-2* 6 days after challenge with isolate A6 containing *AvrMla-12*. Fungal growth is seen as white patches on the leaf surface. Note necrotic (n) areas surrounding infection sites only in *rar1-1* (B). Bar, 200 μm.

(D–L) In situ detection of H_2O_2 by DAB precipitation. The precipitate is restricted subcellularly at sites of attempted fungal penetration 15 hr postinoculation (D–F; bar, 50 μm). Whole-cell H_2O_2 accumulation becomes visible 18 hr after fungal challenge and increases in numbers at single infection sites until approximately 24 hr (G–I; 24 hr postchallenge; bar, 50 μm). Whole-cell DAB staining is restricted to successfully penetrated epidermal cells in *Rar1* sustaining haustoria (J), whereas epidermal cells containing haustoria in *rar1-1* and *rar1-2* show cell wall–associated precipitate only at the site of fungal penetration (K and L). h, haustorium; s, powdery mildew spore; cwa, cell wall apposition. Note DAB staining at CWA in (L). Bar in (J)–(L), 10 μm.

(M–R) Retention of trypan blue 72 hr after fungal challenge. Numerous stained clusters of mesophyll cells were observed only in wild-type *Rar1* plants (M–O; bar, 100 μm). Close-up view of mesophyll cell death is shown in (P). Note that extensive formation of fungal hyphae (fh) occurs only in *rar1-1* and *rar1-2* (Q and R). Arrows indicate sites of mesophyll cell death (mcd). The modified trypan blue infiltration method lead to precipitation of the dye at stomata (st) in all three genotypes. Bar in (P)–(R), 50 μm.

and in all cases the two conserved CHORD domains are arranged in tandem. Mutational analyses of CHORD-encoding genes in both barley and *C. elegans* indicate that *Rar1* represents a *R* gene-dependent signaling component exhibiting molecular commonality across phyla.

Results

rar1 Mutants Are Compromised in Pathogen-Triggered Whole-Cell H_2O_2 Accumulation and Cell Death

Resistant wild-type plants carrying *Rar1* were compared to two susceptible chemically induced allelic mutants, *rar1-1* and *rar1-2*. All three genotypes contain a wild-type allele of the resistance gene *Mla-12* that triggers the resistance response upon challenge with fungal isolate A6, containing *AvrMla-12*. The disease phenotypes of *rar1-1* can be discriminated from *rar1-2* by fewer fungal mycelia, more sparse sporulation, and some necrosis surrounding infection sites 5 to 6 days after pathogen inoculation (Figures 1A–1C).

We have shown previously that the susceptibility of *rar1-1* and *rar1-2* mutants coincides with the inability of epidermal cells to mount a host cell death response (single-cell HR; Freialdenhoven et al., 1994). Because H_2O_2 has been implicated in HR, we asked whether wild-type and mutant *rar1* genotypes differ in their capacity to accumulate H_2O_2 upon pathogen challenge. We used 3,3′-diaminobenzidine (DAB) polymerization to study H_2O_2 accumulation in situ in infected leaf tissues (Figures 1D–1L). DAB is readily taken up by a cut leaf and polymerizes instantly, locally, and in a H_2O_2 dose-dependent manner (Thordal-Christensen et al., 1997).

At 15 hr after fungal spore inoculation, DAB staining was confined to the subcellular cell wall appositions (CWAs) of plant epidermal cells, directly beneath sites of attempted fungal penetration. CWAs are induced in response to fungal attack and may represent a physical barrier against the intruder (Von Röpenack et al., 1998). No differences of DAB staining at CWAs were observed between the three tested genotypes at this early time point (Figures 1D–1F). At 20 hr postinoculation, a brownish DAB precipitate filling the entire penetrated epidermal cell became visible in the wild-type *Rar1* cells, and most of the penetrated cells were darkly stained at 24 hr (Figures 1G and 1J). The number of cells exhibiting whole-cell DAB staining increased until approximately 36 hr after pathogen challenge. Whole-cell DAB polymerization was detected only if the fungus had successfully penetrated into an epidermal cell and had initiated fungal haustorium differentiation (Figure 1J). We recorded a significant reduction in whole-cell DAB staining in both *rar1-1* and *rar1-2* genotypes (*Rar1* had 163 stained cells/cm^2; *rar1-1* had 54 cells/cm^2 and *rar1-2*, 61 cells/cm^2, respectively; Figures 1G–1I). Furthermore, unlike wild-type cells, most epidermal *rar1-1* or *rar1-2* cells containing haustoria lacked whole-cell DAB polymerization (Figures 1K and 1L). In contrast, all three genotypes showed the same frequency of hydrogen peroxide accumulation at CWAs 24 hr postinoculation (Figures 1G–1I). Subcellularly confined DAB staining was also observed adjacent to sites of successful cell wall penetrations in mutants *rar1-1* and *rar1-2* (Figures 1K and 1L). Therefore, neither *rar1* allele compromises the ability of the host to generate H_2O_2 in response to pathogen challenge, but they specifically affect whole-cell H_2O_2 accumulation of attacked epidermal host cells.

We used trypan blue staining to monitor physiological changes in cells destined to die at later stages after fungal spore inoculation (72 and 96 hr postinoculation). Clusters of stained mesophyll cells were only seen in wild type if they subtended attacked epidermal cells (Figures 1M and 1P). Trypan blue clusters were virtually absent beneath emerging fungal colonies in *rar1-2*, whereas occasionally a stained mesophyll cluster could be detected in *rar1-1* (Figures 1N and 1Q). We infer that the host cell death response, triggered by fungal attack, appears to emanate in most cases from epidermal cells that have undergone an HR and spreads into subtending mesophyll tissue.

Map-Based Cloning of *Rar1*

Rar1 was physically delimited within a set of overlapping barley YAC clones bordered by markers MWG876 and Y113R to a maximal size of 630 kb (Figure 2A; Lahaye et al., 1998). BAC sublibraries were established from two of these YAC clones, Y18 and Y30, and a BAC contig was assembled (Figure 2B). Genetic mapping positioned the target gene in centromeric orientation relative to the BAC-derived marker EDDA (Figures 2A and 2B).

Terminal sequences from three BACs (BAC 12, BAC 3H6, and BAC 1B2) were then employed to derive markers OK1114, OK3236, and OK5558, respectively. Each marker cosegregated with *Rar1* (8620 inspected meiotic products segregating for *Rar1*/*rar1* alleles). The target gene was positioned in telomeric orientation relative to three recombination events bordered by Y113R and OK5558. The results obtained by high-resolution genetic mapping combined with a YAC and BAC contig enabled us to narrow down the target interval to a maximal size of 300 kb (interval Y113R-EDDA).

We assembled a contiguous genomic DNA sequence of 65,979 bp covering all markers cosegregating with *Rar1* (OK5558, OK3236, OK1114, and MWG87) except Y18R (Figure 2C). Next we initiated a search for candidate genes in the contiguous 66 kb DNA stretch using the BLAST2 algorithm and available databases. We also tested for intervals exhibiting extended high coding probabilities. ESTs exhibiting relatedness to three distinct regions representing the only predicted possible coding stretches were identified. We designated these intervals I1, I2, and I3 (Figure 2C). Intervals I1 and I2 were similar to each other (59% nucleotide identity) and to aquaporin genes. Interval I3 showed high sequence similarity to a rice EST, C28356, and represented a third coding region in the 66 kb stretch.

Identification of Mutational Events in a *Rar1* Candidate Gene

We compared genomic DNA sequences from wild-type *Rar1* and both *rar1-1* and *rar1-2*, each covering intervals I1, I2, and I3. No sequence polymorphism between the three genotypes was detected for either of the intervals I1 or I2, each covering a length of 3 kb. However, unique

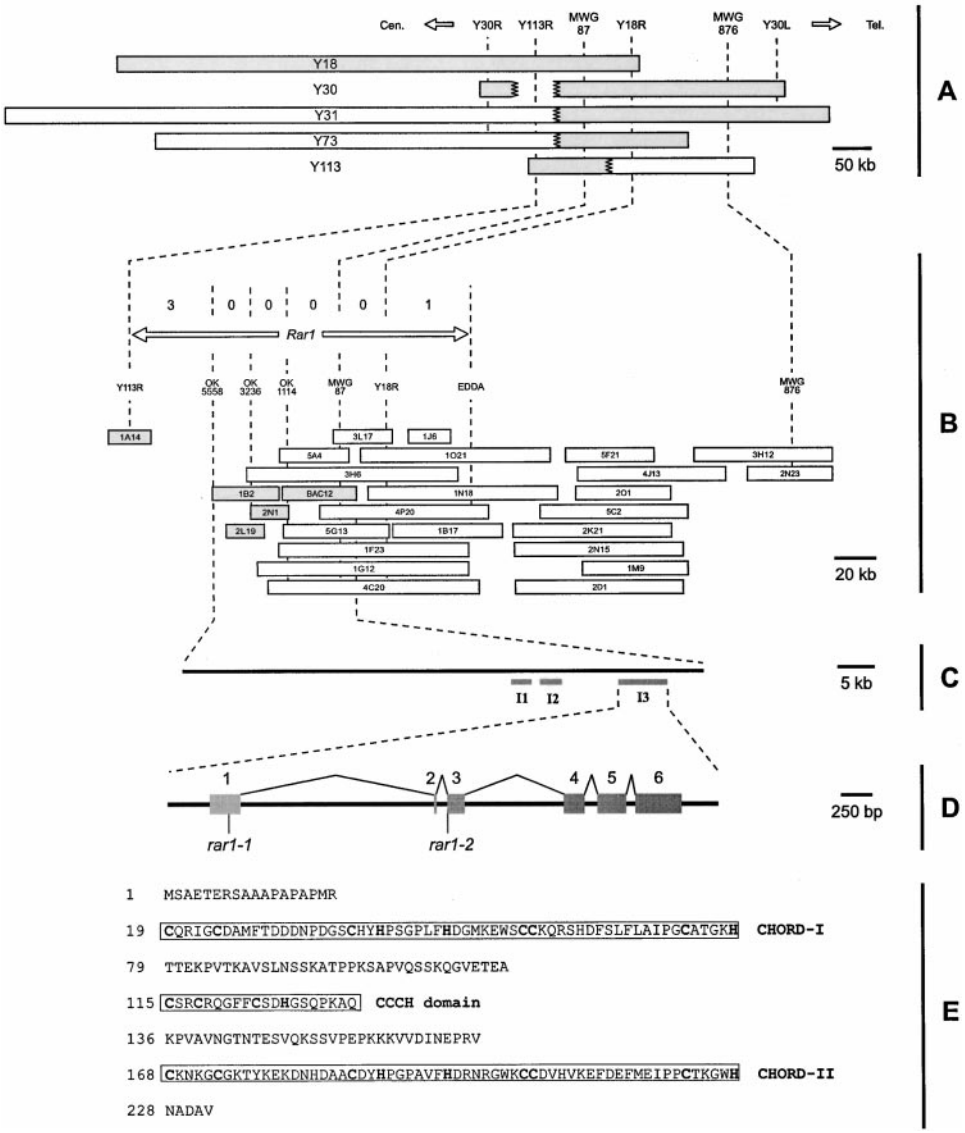

Figure 2. Map-Based Cloning of *Rar1*

(A) Schematic representation of a YAC contig covering the *Rar1* locus. YAC inserts are displayed to scale as bars. Positions of DNA markers are indicated by vertical dashed lines. Stretches that are colinear with the source DNA are highlighted in gray, whereas chimeric parts are displayed in white. An internal deletion in YAC Y30 is indicated. Cen. and Tel. indicate directions to the centromere and telomere of barley chromosome 2H, respectively.

(B) Schematic representation of a BAC contig covering *Rar1*. BAC inserts derived from YACs Y18 and Y30 are displayed to scale as white and gray bars, respectively. Numbers between the vertical dashed lines represent the amount of detected recombinants defined by high-resolution genetic mapping of *Rar1*/*rar1* alleles.

(C) A contiguous sequence stretch at the *Rar1* locus. The black bar depicts the sequenced area. Gray bars indicate regions with high coding probability, which were designated I1, I2, and I3.

(D) *Rar1* gene structure. Exons are highlighted as gray boxes. Positions of mutational events in *rar1-1* and *rar1-2* mutant alleles are indicated. One of the CAPS markers cosegregating with *Rar1*, MWG87, is located between exons 1 and 2.

(E) Deduced amino acid sequence of *Rar1*. Domains CHORD-I (position 19 to 78), CCCH (115 to 134), and CHORD-II (168 to 227) are boxed. Invariant cysteine and histidine residues are indicated in bold letters.

single nucleotide substitutions (both G→A) were discovered in interval I3, at position 56,764 bp for *rar1-1* and position 58,562 bp for *rar1-2*. The finding of mutational events in I3 prompted us to test whether this was a coding region. Primers derived from the I3 interval were then used to isolate a full-length cDNA from leaf RNA. A comparison of genomic and cDNA revealed six exons, each flanked by consensus splice site sequences. Notable is exon 2 consisting of only 3 bp (Figure 1D). The deduced protein of 232 amino acids has a molecular weight of approximately 25.5 kDa (Figure 2E). Lack of detectable transmembrane helices and transit or leader peptide sequences is suggestive of an intracellular localization.

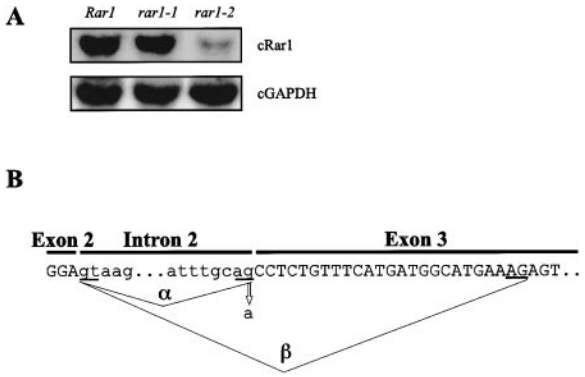

Figure 3. Transcript Analysis of Wild-Type and *rar1* Mutant Alleles

(A) RNA blot analysis of *Rar1* transcript accumulation. Total RNA (50 μg) from 7-day-old uninfected barley leaves of wild-type *Rar1* and mutants *rar1-1* and *rar1-2* were probed with full-length *Rar1* cDNA. The signal corresponds to a size of approximately 1.1 kb. The filter was reprobed with labeled cDNA encoding barley glyceraldehyde-3-phosphate dehydrogenase (cGAPDH) (Martin et al., 1989). Exposure times for autoradiography were 8-fold longer for cRar1 in comparison to cGAPDH.

(B) Schematic representation of splice products detected in *rar1-2* plants. The sequence highlights relevant parts of genomic DNA of exon 2, intron 2, and exon 3 as indicated. Intron sequences are displayed in lowercase letters; exon sequences in uppercase letters. Underlined dinucleotides of lowercase letters denote 5′ and 3′ splice acceptor sites of intron 2, respectively. The underlined dinucleotide in the uppercase letter sequence denotes the cryptic 3′ splice acceptor site utilized in *rar1-2* plants. The arrow marks the mutation detected in genotype *rar1-2* (G→A). α and β denote splicing events resulting in wild-type and mutant cDNA products.

The *rar1-2* Allele Perturbs Splicing and Transcript Accumulation

The base change in genotype *rar1-1* results in a Cys24→Tyr substitution in the deduced 25.5 kDa candidate protein. In contrast, the G→A change identified in genotype *rar1-2* affects an invariant nucleotide within the 3′ splice site consensus sequence of intron 2. The G nucleotide of a 3′ splice site consensus that borders introns is known to be essential for processing of primary mRNA transcripts in both plant and other higher eukaryotic species (Goodall and Filipowicz, 1991). First, we analyzed the steady-state mRNA levels of the candidate gene in wild-type *Rar1* and mutant genotypes by RNA blots. A drastic reduction of transcript levels was observed in genotype *rar1-2* in comparison to *rar1-1* and *Rar1* plants (Figure 3A). To reveal any processing effects, we analyzed mRNA species corresponding to the candidate gene in genotype *rar1-2* by RT–PCR. Sequencing of 20 cloned cDNA products revealed two classes, one identical to the wild-type *Rar1* cDNA and another lacking 25 bp in exon 3 immediately downstream of the G→A transition (Figure 3B). Inspection of genomic DNA revealed, within exon 3, a cryptic splice site (AG) 25 bp downstream from the mutated 3′ splice consensus. The deletion in the cDNA of genotype *rar1-2* thus alters the reading frame, which, in turn, leads to a truncation of the protein due to a stop codon within exon 5. Thus, the splice site mutation in the candidate gene of mutant *rar1-2* leads both to an aberrantly spliced transcript and a reduction of steady-state mRNA levels. In conclusion, the finding of two mutational events in genotypes *rar1-1* and *rar1-2*, which lead either to protein or mRNA defects of a candidate gene in the physically delimited target interval, indicated that we isolated *Rar1*.

Rar1 Contains a Novel Eukaryotic Protein Domain: CHORD

Analysis of the Rar1 protein sequence did not reveal any significant homologies to previously characterized proteins. However, a close inspection indicated the presence of two 60 aa long repeated motifs at the N and C terminus, comprising 51% of the predicted full-length protein (Figure 2E). Inspection of EST databases uncovered a number of cDNAs from eukaryotic species sharing significant similarity to the 60 aa sequence blocks in barley Rar1. In addition, related sequences were identified in genomic sequences from *Arabidopsis* and the nematode *C. elegans*. Isolation of corresponding cDNAs by RT–PCR and DNA sequencing confirmed their relatedness to the 60 aa barley Rar1 sequence motif. Assembly and comparison of deduced full-length protein sequences of barley *Rar1*-related genes from *Arabidopsis*, *Toxoplasma*, *C. elegans*, *Drosophila*, and human uncovered the same tandem organization of the 60 aa motif as well as similar spacing (64 to 92 aa) in each species (Figure 4A).

Alignment of Rar1-related protein sequences from the tested phyla revealed that the sequence conservation is restricted to the tandem blocks of 60 aa. A closer inspection of the aligned sequences showed that six cysteine and two histidine residues are invariant within the 60 aa motif (Figure 4B). Three other residues within the tandem blocks are also invariant and some positions are confined to positive, negative, or aromatic amino acids. We have designated this novel protein cassette CHORD and the N- and C-terminal versions as CHORD-I and CHORD-II, respectively. Interestingly, the Cys24→Tyr substitution identified in barley mutant *rar1-1* affects one of the invariant cysteine residues in CHORD-I.

Rar1 homologs were also isolated from diverse plant species; rice, maize, and *Brassica* (data not shown). Sequence alignment of the predicted plant Rar1 proteins revealed an additional highly conserved 20 aa sequence motif (95%–100% sequence identity), which is absent in all tested nonplant species. We designated this stretch CCCH because it contains an additional set of three invariant cysteine and a histidine residue (Figure 2E). In contrast, *Drosophila*, *C. elegans*, and human have acquired a C-terminal extension adjacent to CHORD-II. Interestingly, this C-terminal extension shares significant sequence similarity with Sgt1, which was recently shown to be essential for activation/assembly of the ubiquitin ligation machinery (SCF) and the kinetochore complex (CBF3) in yeast (Figure 4C; Kitagawa et al., 1999). In *C. elegans*, this motif is present only in the CHORD-containing protein and the Sgt1 homolog. We designated this motif CS after *C*HORD-containing proteins and *S*gt1.

CHORD Binds Zn^{2+} Ions

The striking conservation of cysteine and histidine residues within CHORD, in combination with the predicted intracellular location of the deduced protein, suggested that Rar1 may bind metal ions. To test this, we expressed

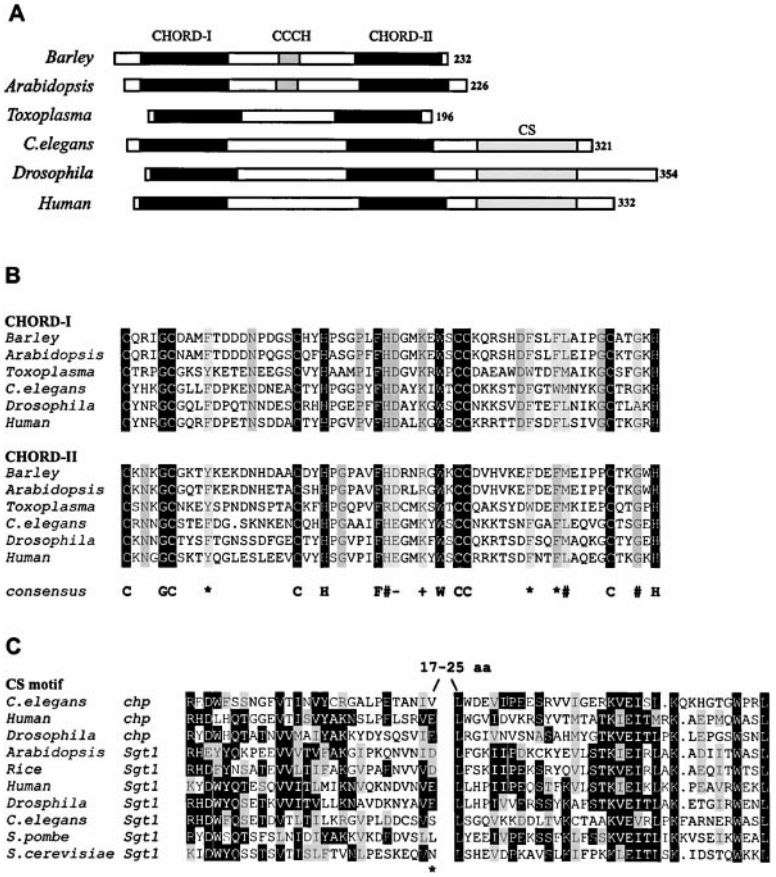

Figure 4. Graphic Representation and Sequence Alignments of CHORD Proteins

(A) Graphic representation of proteins containing CHORD domains from barley, *Arabidopsis*, *Toxoplasma*, *C. elegans*, *Drosophila*, and human. Black boxes represent either CHORD-I or -II as indicated. Gray boxes represent the 20–amino acid CCCH motif. Numbers given on the right refer to the amino acid length of each deduced protein.

(B) Amino acid sequence alignment of CHORD domains from various species. Black boxes highlight invariant amino acid in both CHORD-I and -II; dark gray shading indicates identical amino acids in either CHORD-I or -II; light gray boxes indicate >50% identity through conservative amino acid substitutions in both CHORD-I and -II. In the consensus shown, an asterisk indicates aromatic residues, a pound sign indicates highly conserved residues, a minus sign designates negatively charged residues, and a plus sign designates positively charged residues.

(C) Amino acid sequence alignment of the CS motif. Identical and similar residues are displayed in black and gray boxes, respectively. The asterisk marks the position of the *sgt1-3* mutation.

full-length *Rar1* and *rar1-1* as well as truncated versions containing CHORD-I or CHORD-II in *E. coli*. Each of these proteins was expressed as a C-terminal fusion to the 15–amino acid S-TAG peptide (Kim and Raines, 1994). Four S-TAG fusion proteins, S-TAG::Rar1, S-TAG::rar1-1, S-TAG::CHORD-I (M^1-V^{110}), and S-TAG::CHORD-II (S^{150}-V^{232}), were purified to near homogeneity by affinity chromatography (Figures 5A and 5B). In a first set of experiments, we carried out a multi–metal ion analysis by using simultaneous/sequential inductively coupled plasma atomic emission spectroscopy (ICP-AES). Out of five tested metal ions (Fe^{3+}, Zn^{2+}, Mn^{2+}, Ni^{2+}, and Cu^{2+}), only Zn^{2+} associated with the S-TAG::Rar1 and S-TAG::rar1-1 fusion proteins (Table 1). From independent experiments, we calculated for both derivatives between 1.4 to 2.3 mole equivalents of Zn^{2+}.

In a second set of experiments, we measured Zn^{2+} binding of the Rar1 derivatives by a colorimetric assay based on complex formation with 4-(2-pyridylazo) resorcinol (PAR). Whereas essentially no Zn^{2+} was found associated with BSA as a negative control, S-TAG::Rar1 and S-TAG::rar1-1 were found to contain very similar mole equivalents of Zn^{2+} (1.46 and 1.36, respectively; Table 1). Both S-TAG::CHORD-I and S-TAG::CHORD-II derivatives retained Zn^{2+} binding, but the mole equivalents were considerably lower compared to the full-length Rar1 fusion proteins. The sum of Zn^{2+} equivalents detected in S-TAG::CHORD-I and S-TAG::CHORD-II corresponds approximately to the mole equivalents detected in the full-length derivatives (Table 1). Control experiments with the chelating agent EDTA (10 mM) prior to the PAR assay depleted each purified S-TAG::Rar1 derivative from Zn^{2+} below the level of detection. These data show that both CHORD-I and CHORD-II can function as autonomous Zn^{2+} coordinating domains. We

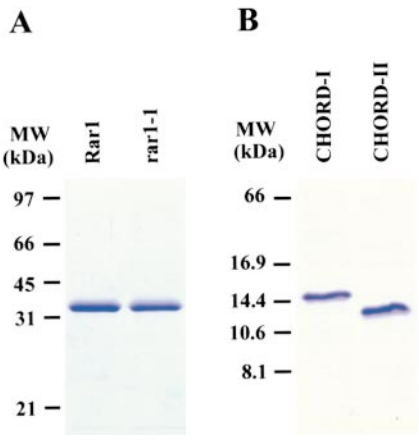

Figure 5. Purification of S-TAG::Rar1 Fusion Proteins

(A) Glycine-SDS-PAGE (12%) analysis of S-TAG::Rar1 and S-TAG::rar1-1 full-length fusion proteins after purification by ribonuclease S-protein agarose affinity chromatography. Size standards indicated in kilodaltons.

(B) Tricine-SDS-PAGE (10%) analysis of S-TAG::CHORD-I and S-TAG::CHORD-II fusion proteins after purification by ribonuclease S-protein agarose affinity chromatography. Size standards indicated in kilodaltons.

Table 1. Zn^{2+} Content of S-TAG::Rar1 Fusion Proteins

	ICP-AES Analysis[a]	PAR Assay[a]
S-TAG::Rar1	2.02/2.33	1.50/1.47/1.42
S-TAG::rar1-1	2.08/1.36	1.25/1.13/1.53
S-TAG::CHORD-I	1.16/0.72	0.60/0.75
S-TAG::CHORD-II	1.29/1.40	0.99/1.00
BSA	NT[b]	0.10

Zn^{2+}/protein (mole equivalents). Protein concentration was measured by BCA assays.

[a] The numbers indicated refer to results from independent experiments.

[b] NT, not tested

conclude that each domain has the capacity to bind at least 1 mole equivalent of Zn^{2+}.

Silencing *chp*, the CHORD Homolog in *C. elegans*

To find out whether CHORD proteins have overlapping functions across phyla, we silenced the *Rar1* homolog in *C. elegans*, designated *chp* (*CH*ORD *p*rotein), by RNA interference technology (RNAi) (Fire et al., 1998). We found that RNAi of *chp* in the injected worm resulted in both reduction of fecundity and increased embryo lethality (Tables 2 and 3; Figures 6A and 6B). Egg production of injected worms [*chp* (RNAi) P_o] was 30%–40% of the level produced by water or *apx-1* injected control hermaphrodites [H_2O P_o]. The rate of egg production by *chp* (RNAi) P_o animals was measured over time (Figure 6A). The number of eggs laid per hour was reduced by at least 2-fold compared to the H_2O P_o animals. A reduction of hatching was observed 24 hr postinjection but was more pronounced among eggs laid 32 hr postinjection (Figure 6B). The marginal reduction observed at the earlier time point could be due to residual *chp* function supplied by the mother.

Silencing of *chp* by RNAi also caused animals to die early in embryogenesis; none of the unhatched embryos reached the comma stage of development. Among the 40% of the embryos that hatched, 98% (n = 531) developed into adults. The remaining 2% arrested at the L1 stage and died. Among the F1 progeny of the injected animals [*chp-1* (RNAi) F1] that developed into adults, 3%–5% had a protruding vulva phenotype (Pvl; Figure 7A), about 1% had two vulva (Muv; Figure 7B), and another 1% showed varying degrees of deformities. There were also more animals bursting at the vulva compared to F1 progeny of water-injected animals (data not shown). Otherwise, the animals looked normal. Consistent with the carryover effect of RNA interference, brood size of *chp* (RNAi) F1 animals was reduced to about 40% of wild type (Table 3).

Apart from the semisterility phenotype, we observed that many of the *chp* (RNAi) F1 animals showed germline defects. In adult *chp* (RNAi) F1 hermaphrodites, both gonad arms were usually present, and the distal arms look normal. In rare cases (<5%), one gonadal arm was missing and the uterus appeared to be more vacuolated (Figure 7A). However, in many adult *chp* (RNAi) F1 animals, the proximal arms were strikingly disorganized. Instead of a single file of full-sized oocytes, they were filled with large numbers of small cells, similar to those in the distal arms (Figures 7C and 7D). This gonad hyperplasia is reminiscent of *ced-3* and *ced-4* mutants, which fail to execute PCD in about half of female germ cells (Gumienny et al., 1999). These observations suggest a defect in oogenesis and/or oocyte maturation, which may explain the semisterility phenotype of these animals.

Discussion

Whole-Cell H_2O_2 Accumulation Is *Rar1* Dependent

Biphasic increases of H_2O_2 have been reported in several cultured plant cell systems in response to bacterial or fungal *Avr* genes (Levine et al., 1994). In these systems, a first peak usually occurs within the first hour and a second, sustained peak occurs 4–5 hr later. The first peak has been interpreted as nonspecific because it was induced by both virulent and avirulent bacteria, whereas the second sustained burst was considered to be race specific. An alternative model suggests that biphasic ROI accumulation is an intrinsic property of pathogen-challenged plant cells, with a first minor burst being required to potentiate a second, sustained ROI production (Shirasu et al., 1997). Strikingly, the biphasic accumulation profiles of H_2O_2 in challenged cultured cell systems parallels a spatial and temporal accumulation pattern seen, in this study, at the site of attempted penetration (CWAs) and subsequently in whole attacked cells. Our histochemical analysis shows that mutations in *Rar1* interfere with whole-cell H_2O_2 accumulation, but not with its accumulation at CWAs, which contain arrested fungal penetration attempts. The two accumulation phases are separated by at least 5 hr. The second *Mla-12*-triggered and *Rar1*-dependent oxidative burst

Table 2. Fertility and Embryonic Viability of Injected Worm

			Phenotype of the Injected Worm			
Strain	dsRNA Injected	n[a]	No. of Eggs Laid/Worm (± SE)	p Value[b]	Percentage of Viable Eggs (± SE)	p Value[b]
Wild type	Water	10	258.0 ± 8.7		98.9 ± 0.7	
Wild type	*chp-1*	15	85.9 ± 5.9	<0.0001	41.2 ± 4.1	<0.0001
Wild type	*apx-1*[c]	7	220.7 ± 15.9	0.051	0.0	<0.0001

[a] Total number of animals injected. Numbers represent the summary of at least two separate injections performed on separate days.

[b] p value from Mann-Whitney U test performed using Statview 5.0.

[c] Injection with *apx-1* dsRNA was used as a positive control. *apx-1* dsRNA results in total failure of eggs to hatch but has no significant effect in fecundity.

Table 3. Fertility of F1 Progeny

		Fertility of F1 Progeny of Injected Animals		
		n[a]	Brood Size/Worm (± SE)	p Value[b]
Wild type	Water	24	351.0 ± 5.7	
Wild type	*chp-1*	35	144.1 ± 14.6	<0.0001

[a] Total number of F1 progeny of injected animals.
[b] p value from Mann-Whitney U test performed using Statview 5.0.

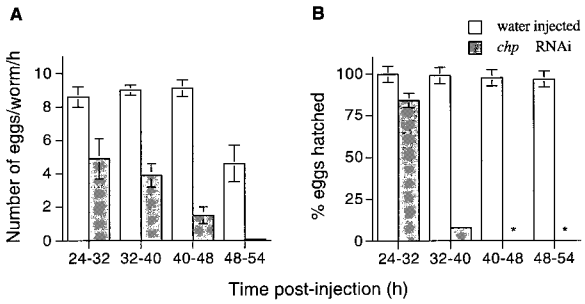

Figure 6. Time Course Analysis of Egg Production and Viability in *C. elegans*

(A) Rate of egg production (y axis) by animals injected with water or with double-stranded *chp* RNA at various time points postinjection (x axis).

(B) Viability of eggs (% hatched, y axis) produced by animals injected with water or with double-stranded *chp* RNA at various time points postinjection (x axis).

occurs postpenetration, coincident with fungal haustorium differentiation. Differences in the time lag between the onset of oxidative bursts in challenged cultured cells and in mildew-infected leaves may be reflected by the time needed to transfer the fungal *Avr* signal to the host cell. The data reported here imply that *Rar1* must function upstream of a whole-cell hydrogen peroxide burst within attacked epidermal cells.

Signals Causing Cell Death Cross Tissue Borders in a *Rar1*-Dependent Manner

Resistance, triggered by *Mla-12* and dependent on *Rar1*, correlates with a single-cell epidermal HR and is recognizable by whole-cell autofluorescence (Freialdenhoven et al., 1994). This hypersensitive cell death was not detected during the first 24 hr postinoculation of the fungus but was seen thereafter with increasing frequency at single interaction sites up to 48 hr. The number of cells undergoing HR is reduced to background levels in mutants of either *Mla-12* or *Rar1* (Freialdenhoven et al., 1994). Our trypan blue retention experiments revealed a communication between epidermal and underlying mesophyll tissue as part of the resistance response, although only the epidermal tissue is in physical contact with the fungus. Cell death in mesophyll tissue occurred between 48 and 72 hr postinoculation in wild-type leaves, suggesting that cell death signals emanate from the epidermal cell attacked first. Both *rar1* mutants were shown to be compromised in mesophyll cell death. It is tempting to speculate that ROI, generated in the attacked epidermal cell and dependent on *Rar1*, are also involved in spreading a cell death signal from cell to cell into mesophyll tissue. Indeed, DAB polymerization has been also observed in mesophyll cells in *Mla-3* and *Mla-12* specified resistance (Thordal-Christensen et al., 1997; Hückelhoven et al., 1999). Mesophyll staining is mainly confined to the cell walls in the attachment zone

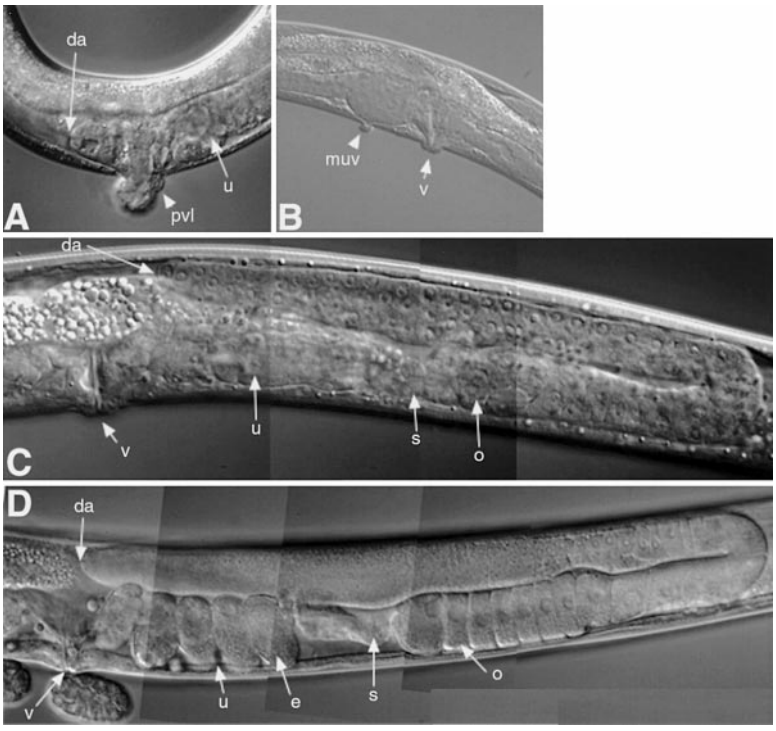

Figure 7. Nomarski Photomicrographs of Adult Hemaphrodite *C. elegans* Showing Vulval, Gonadal, and Germline Defects due to Silencing of *chp*

(A) A *chp* (RNAi) F1 worm showing the protruding vulva (pvl) phenotype. The anterior gonad failed to develop, and the distal arm (da) in this worm failed to extend. Compare the distal arm (da) of the water-injected (H_2O) F1 (D) animal. In addition, the uterus (u) is vacuolated.

(B) The multivulva phenotype of a *chp* (RNAi) F1 worm. In all cases (n = 7), only one additional pseudovulva (muv) was seen.

(C and D) Germline within the posterior gonad of a *chp* (RNAi) F1 (C) and a (H_2O) F1 (D) animal. Note that although the gonad, spermatheca (s), and vulva (v) of the *chp* (RNAi) F1 (C) appear normal, the oocytes (o) at the proximal arm are much smaller and disorganized compared to the single file arrangement of the large oocytes in the (H_2O) F1 (D) animal. In addition, no normally developing eggs (e) are present in the uterus (u) of this *chp* (RNAi) F1 animal (C).

between epidermal and mesophyll cells. Moreover, a functional contribution of mesophyll tissue to the *Mla-12* triggered resistance response is supported by the failure of dissected epidermal monolayers to confer fungal growth arrest (Schiffer et al., 1997).

CHORD, a Novel Eukaryotic Zn^{2+}-Binding Domain

Molecular isolation of *Rar1* uncovered the 60 aa CHORD motif. CHORD-containing proteins were discovered in all lower and higher eukaryotes examined, except yeast. Southern blot analysis with DNA from multiple plant species and the complete genome sequence of *C. elegans* show that CHORD proteins are generally encoded by single-copy genes (data not shown). The string of invariant cysteine and histidine residues both in CHORD-I and CHORD-II is a notable feature within the sequence motif. Their functional relevance is strongly supported by the *rar1-1* allele, where Cys-24 within CHORD-I is changed to a tyrosine. Our biochemical experiments provide direct evidence that CHORD-I and CHORD-II function as autonomous Zn^{2+}-binding domains. This is consistent with the predicted intracellular location of barley Rar1 and the identified homologs in other species. To date, a total of ten "zinc finger" topologies have been described (Schwabe and Klug, 1994). Each of these has a different consensus from the C-x4-C-x12-13-C-x2-H-x14-CC-x15-C-x4-H signature of CHORD. However, the number of invariant cysteines and histidines that may function as Zn^{2+} ligands in CHORD is identical to that of the "double-zinc finger" domains such as RING, LIM, and PHD/LAP (Borden and Freemont, 1996). Based on the number of potential Zn^{2+} ligands, CHORD may be a member the double-zinc finger subfamily. However, our analysis of full-length Rar1, CHORD-I, and CHORD-II fusion proteins shows that each CHORD binds probably one mole equivalent of Zn^{2+}. Thus, it is likely that only some of the potential ligands in CHORD coordinate Zn^{2+}.

It is well known that single ligand substitutions within zinc fingers can result in retained zinc binding but impaired protein function due to local conformational perturbation (Webster et al., 1991). Thus, it remains possible that Cys-24 in CHORD-I is involved in Zn^{2+} binding. In this case, the weakly defective *rar1-1* phenotype may result from a subtle change in protein conformation. Another interesting feature of CHORD is the presence of three additional invariant residues (Gly, Phe, and Trp) as well as 11 residues conserved in charge or hydrophobicity. Similarly, LIM domains also have a substantial conservation of other residues in addition to the essential metal-binding sites (Sanchez-Garcia and Rabbitts, 1994), but none of these are invariant.

A Model for *Rar1* in Mediating *R* Gene Activity

Individual CHORD domains from different species can be unambiguously assigned to either CHORD-I or CHORD-II. If domains I and II are involved in similar or identical functions within the same protein, then one would expect that they diverge in sequence during evolution with similar rates but leave the same critical amino acids unaltered. For example, this scenario should make it difficult to assign the two human CHORD sequences unambiguously to domains I and II of *Toxoplasma*. However, corresponding CHORD domain sequences from different phyla are more closely related than CHORD-I and CHORD-II sequences within the same protein (Figure 5B). This is suggestive of discrete functions for CHORD-I and CHORD-II. Similar observations have been made for particular LIM domains in proteins containing more than one LIM copy (Gill, 1995). In a simplistic view, a bifunctional model for CHORD proteins would be compatible with the deduced genetic position of *Rar1* in a pathway controlling pathogen resistance. In this model, one CHORD would have the capacity to perceive upstream signals triggered by a number of different R proteins, and the other would interact with downstream components, possibly leading to the activation of a sustained oxidative burst, resistance, and cell death. Alternatively, both CHORD-I and CHORD-II could function as a single functional unit.

Genetic tests have shown that *Rar1* is not only required for the function of multiple resistance specificities encoded at a single resistance locus (*Mla*) but also for other unlinked powdery mildew *R* loci (Jørgensen, 1996). Recently, the *Mla* locus has been shown to contain several genes each encoding NBS-LRR type R proteins (Wei et al., 1999). To date, only two genes representing converging points in race-specific resistance to pathogens have been molecularly characterized from plants. Both are from the dicot *Arabidopsis*. *NDR1* encodes a small and possibly membrane-anchored protein with unknown function, and *EDS1* encodes an intracellular protein containing three sequence motifs characteristic of lipases (Century et al., 1995; Falk et al., 1999). *NDR1* and *EDS1* are plant specific, whereas homologs of barley *Rar1* exist in all eukaryotic species examined, except yeast. For both NDR1 and EDS1 proteins, it is not known whether they represent common signaling or common effector components of multiple *R* genes. It is also unknown whether they act upstream or downstream of the oxidative burst preceding HR. Null mutants in *NDR1* or *EDS1* preferentially compromise the action of different subfamilies of the NBS-LRR *R* gene class (Aarts et al., 1998). Similarly, *rar1* alleles affect only a subset of barley powdery mildew *R* genes (Jørgensen, 1996). However, since both *rar1-1* and *rar1-2* are not null mutants, it is possible that many other *R* genes are still fully functional due to residual Rar1 activity in those alleles.

CHORD: Common or Different Functions across Phyla?

Reducing the levels of the CHORD protein in *C. elegans* by RNA interference caused semisterility in the adult hermaphrodites and lethality of embryos. The semisterility correlated with specific defects in germline development. The other phenotypes observed included larval lethality and defects in vulval development. As *chp* is a single-copy gene in *C. elegans*, we are confident that the *chp* (RNAi) phenotypes reflect a loss of function of *chp*. Together, our data suggest that CHP plays a vital role in germline development and embryogenesis.

At present, two contrasting models can be deduced for CHORD protein function(s). The first model assumes different functions in plants and metazoans. This would be supported by the presence of the CCCH motif in

plants and the CS domain in insects and mammals. Similarly, the phenotypes of *rar1* defective alleles in barley and *chp* (RNAi) in *C. elegans* appear at first to be unrelated. The second model suggests common or at least overlapping functions of CHORD proteins across phyla. The lack of copy number expansion of CHORD proteins within a species and the strict conservation of tandem organization of CHORDs across phyla suggest that the CHORD-I/CHORD-II tandem array is not merely a structural motif but more likely a unit of conserved function.

Only metazoan CHORD proteins contain the CS motif, exclusively shared with the SCF/CBF3 complex activator Sgt1 (Kitagawa et al., 1999). Both Sgt1 and CHORD proteins are highly conserved across eukaryotic phyla. It is possible that Sgt1 and CHP have a common function defined by the CS motif. Although the function of the CS motif in Sgt1 is still unknown, it should be noted that one of the mutations in a temperature-sensitive allele, *sgt1-3*, was found in this motif (Figure 4C; Kitagawa et al., 1999). Since *sgt1-3* cells are defective in the formation of CBF3 complex, the CS motif may be required for this function. An alternative interpretation is based on the finding that some pairs of interacting domains, each in separate proteins of one organism, have homologs in another organism fused into a single polypeptide chain (Marcotte et al., 1999). The fact that CHORD and the CS domain are fused into a single polypeptide chain in metazoans but are found in separate proteins in plants may be indicative of an interaction between CHORD and CS. This may provide a link of CHORD proteins to SCF/CBF3 complex formation.

The ubiquity of cell death in *R* gene–dependent resistance in plants to obligate biotrophic fungi suggests it is programmed (Pennell and Lamb, 1997). Recent data in *C. elegans* provided clear evidence for programmed cell death in the germline (Gumienny et al., 1999). Germline and somatic cell death utilize the same execution machinery (*ced-3*, *ced-4*, and *ced-9*) but a distinct activation pathway. One of the phenotypes of adult *chp* (RNAi) F1 animals, namely disorganization and filling of the proximal tubular arms with large numbers of small cells (Figure 7C), is strikingly similar to the reported female germline hyperplasia in *ced-3* and *ced-4* mutants (Gumienny et al., 1999). Consistent with this, the germline hyperplasia phenotype in adult *chp* (RNAi) F1 appears to be restricted to the female germline, since *chp* RNAi in a *him-8* mutant background did not show any detectable defect compared to *him-8* males from water-injected controls (data not shown). It will be necessary to isolate *chp* mutants to find out whether the wild-type gene exerts overlapping functions with the control of programmed cell death in the female germline or perturbs oogenesis by a different mechanism.

We have concluded that *rar1-1* and *rar1-2* are not null mutants. This and the fact that mutants in *Rar1* were isolated with a 10-fold lower frequency compared to mutations in the *R* gene *Mla-12* (Torp and Jørgensen, 1986) suggest that *Rar1* may have an essential cellular function. Thus, if null mutants of barley *Rar1* are lethal, then *rar1-1* and *rar1-2* may compromise only a subfunction of the wild-type protein. This subfunction is the *R* gene–triggered recruitment of an evolutionary conserved and essential cellular component to initiate resistance and cell death. The other function may be revealed by the isolation and characterization of *rar1* null mutants, which we are currently pursuing in *Arabidopsis*. Future functional studies of CHORD proteins in multiple species may reveal not only the role of *Rar1* in plant/pathogen interactions, but also its general role in common mechanisms controlling cell death and development across species.

Table 4. CAPS Markers

Marker	Primer	Restriction Enzyme
OK1114	CCATGTCTTGTCCATGATGCACC	HindIII
	GCCATCTAGCTACTAACTATGGACCCG	
OK3236	GACAGTAGCAGAGTGGTTGCACCG	
	CCACATGCACACAAGTATATGCACAC	
OK5558	GCGATATGGAGATCAAAACCCTCA	
	CACGAAATGCCTATGAACCATTCG	
EDDA	ACTTTAAACTTGCTGGCGACAAGAGAC	BfaI
	GGAGTTGGCTTACTTACCGTATCACATAC	

Experimental Procedures

Plant Material, Fungal Isolates, and Infection Procedures

Seeds of doubled-haploid barley (*Hordeum vulgare*) line Sultan5 (*Mla-12 Rar1*) and mutants M82 (*Mla-12 rar1-1*) and M100 (*Mla-12 rar1-2*) were generously provided by J. Helms Jørgensen, Riso National Laboratory, Risø, Denmark (Torp and Jørgensen, 1986). Powdery mildew infections were performed in a phytochamber with *Erysiphe graminis* f sp *hordei* isolate A6 expressing *AvrMla-12* (Freialdenhoven et al, 1994). The inoculation density was controlled at approximately 50 spores/mm^2.

Histochemical Analysis

Uptake of DAB (3,3′-diaminobenzidine; 1 mg/ml; Sigma) by barley primary leaves was carried out as described previously (Thordal-Christensen et al., 1997). Trypan blue retention was performed as described (Peterhänsel et al., 1997).

BAC Contig Assembly, Genetic Mapping, and DNA Manipulation

BAC sublibraries from YAC clones Y18 and Y30 (Lahaye et al., 1998) were constructed by partial digestion of total yeast DNA with HindIII and ligating size-fractionated DNA fragments with an average size of 50 to 100 kb into vector pBeloBAC11 (Bendahmane, 1999). CAPS markers, Y113R, MWG87, Y18R Y73L, MWG876, and Y30L were used to identify BAC clones containing the *Rar1* locus. Terminal insert sequences of these BAC clones were subsequently determined to generate PCR-based markers (Table 4). The contiguous nucleotide sequence of BAC12 and 1B2 was determined by standard shotgun sequencing procedures. To identify 5′ and 3′ ends of the *Rar1* cDNA, a barley RACE library was constructed using the MARATHON cDNA amplification kit (Clontech).

RNA Interference

The template for the sense and antisense *chp* RNA transcripts was obtained from the full-length *chp* cDNA subcloned into pGEM T EASY (Promega) using the MEGAscript T7 and SP6 kit (Ambion). The sense and antisense RNA were mixed in equal concentrations of 5 μg/μl and injected into the gut of L4 hermaphrodites. Animals were allowed to recover for 24 hr at 20°C. Viable injected animals [designated *chp-1* (RNAi) P_o] were transferred singly every 6–10 hr to fresh plates and allowed to lay eggs at 20°C. Broods were scored for dead eggs 1 day post–egg lay, and for L4 larvae or adults 2 days post–egg lay. Phenotypes of the F1 animals [*chp-1*(RNAi) F1] were determined by visualizing through a dissecting scope or a Zeiss Axioplat microscope (Carl Zeiss) equipped with polarizing optics.

Fertility of the *chp-1*(RNAi) F1 animals was determined by transferring a subset of the animals at the L4 stage to fresh plates for egg lay at 20°C every 24 hr, until no more eggs were produced. Larvae were scored 24 hr after removal of the *chp-1*(RNAi) F1 adult.

Overexpression and Affinity Purification of S-TAG Fusion Proteins

Plasmids overexpressing S-TAG fusion proteins of full-length Rar1, CHORD-I, or CHORD-II were constructed in-frame using unique BamHI (Rar1) or EcoRI (CHORDs) sites within pSTAG (kindly provided by C. Martin; Edwards et al., 1999). The *rar1-1* mutation was reconstructed using the splicing by overlap extension method (Horton et al., 1989). These plasmids were introduced into *E. coli* strain BL21 harboring p*Lys*S and pSBET, which express T7 lysozyme and *arg*U, respectively, to maximize expression levels (Edwards et al., 1999). Freshly transformed bacterial cells were inoculated in L medium containing 1 μM zinc chloride and incubated at 30°C up to A_{600} values of approximately 0.6. IPTG was then added to the culture (1 mM), and the incubation was continued for 1 hr. IPTG-treated cells were harvested and sonicated in the binding buffer (20 mM Tris-HCl [pH 7.5], 150 mM NaCl, 1% Triton X-100.) The filtered supernatant was directly loaded on an S-protein agarose column (Novagen, Madison). After an extensive wash with the binding buffer, the S-TAG fusion proteins were eluted with the binding buffer containing 3 M $MgCl_2$. The fusion proteins were then dialyzed extensively against TNG buffer (10 mM Tris-HCl [pH 8.0], 0.2 M NaCl, and 5% w/v glycerol) for subsequent PAR assays (Giedroc et al., 1986) or against HEPES buffer (pH 7.5) for ICP-AES analysis (Southern Water, Brighton, UK).

Protein concentration was determined by BCA assays (Pierce, Rockford, IL). Proteins were separated either by 10% tricine-SDS–PAGE or by 12% glycine-SDS–PAGE and subsequently visualized by Coomassie brilliant blue staining.

Source of EST Clones Containing *Rar1* Homologs

Toxoplasma gondii EST clone tgzy47d08, *Drosophila melanogaster* EST clone CK76, and Rice Sgt1 Est clone C62803 were obtained from Genome Systems Inc. (St. Louis, MO.), the Berkeley Drosophila Genome Project (Berkeley, CA), and MAFF DNA Bank (Tsukuba, Japan), respectively. Human EST clones 148205, 187178, 159148, and 189934 were obtained from American Type Culture Collection (Manassas, VA).

Acknowledgments

This paper is dedicated to Prof. Francesco Salamini on the occasion of his 60th birthday. We thank Margaret Shailer for technical assistance and our colleagues Desmond Bradley and Jonathan Jones for critical reading of the manuscript. This work was supported by grants from the GATSBY Charitable Foundation and the BBSRC to P. S.-L.

Received February 26, 1999; revised September 30, 1999.

References

Aarts, N., Metz, M., Holub, E., Staskawicz, B.J., Daniels, M.J., and Parker, J.E. (1998). Different requirements for *EDS1* and *NDR1* by disease resistance genes define at least two R gene-mediated signaling pathways in Arabidopsis. Proc. Natl. Acad. Sci. USA *95*, 10306–10311.

Baker, B., Zambryski, P., Staskawicz, B., and Dinesh-Kumar, S.P. (1997). Signaling in plant-microbe interactions. Science *276*, 726–733.

Bendahmane, A. (1999). Zero-background plasmid vector for BAC library construction. Biotechniques, in press.

Borden, K.L. B., and Freemont, P.S. (1996). The RING finger domain: a recent example of a sequence-structure family. Curr. Opin. Struct. Biol. *6*, 395–401.

Century, K., Holub, E., and Staskawicz, B.J. (1995). *NDR1*, a locus in *Arabidopsis thaliana* that is required for disease resistance to both a bacterial and fungal pathogen. Proc. Natl. Acad. Sci. USA *92*, 6597–6601.

Dietrich, R.A., Delaney, T.P., Uknes, S.J., Ward, E.R., Ryals, J.A., and Dangl, J.L. (1994). Arabidopsis mutants simulating disease resistance response. Cell *77*, 565–577.

Edwards, A., Borthakur, A., Bornemann, S., Venail, J., Denyer, K., Waite, D., Fulton, D., Smith, A., and Martin, C. (1999). Specificity of starch synthase isoforms from potato. Eur. J. Biochem., in press.

Falk, A., Feys, B., Frost, L., Daniels, M., and Parker, J. (1999). The *Arabidopsis EDS1* gene encodes an essential component of *R* gene-specified disease resistance that has similarity to lipases. Proc. Natl. Acad. Sci. USA *95*, 10306–10311.

Fire, A., Xu, S.Q., Montgomery, M.K., Kostas, S.A., Driver, S.E., and Mello, C. C. (1998). Potent and specific genetic interference by double-stranded RNA in *Caenorhabditis elegans*. Nature *391*, 806–811.

Freialdenhoven, A., Scherag, B., Hollricher, K., Collinge, D.B., Thordal-Christensen, H., and Schulze-Lefert, P. (1994). *Nar-1* and *Nar-2*, two loci required for *Mla12*-specified race-specific resistance to powdery mildew in barley. Plant Cell *6*, 983–994.

Giedroc, D.P., Keating, K.M., Williams, K.R., Konigsberg, W.H., and Coleman, J.E. (1986). Gene 32 protein, the single-stranded DNA binding protein from bacteriophage T4, is a zinc metalloprotein. Proc. Natl. Acad. Sci. USA *83*, 8452–8456.

Gill, G.N. (1995). The enigma of LIM domains. Structure *3*, 1285–1289.

Goodall, G.J., and Filipowicz, W. (1991). Different effects of intron nucleotide composition and secondary structure on pre-mRNA splicing in monocot and dicot plants. EMBO J. *10*, 2635–2644.

Greenberg, J.T., Guo, A., Klessig, D.F., and Ausubel, F.M. (1994). Programmed cell death in plants: a pathogen-triggered response activated coordinately with multiple defense functions. Cell *77*, 551-563.

Groom, Q.J., Torres, M.A., Fordham-Skelton, A.P., Hammond-Kosack, K.E., and Jones, J.D.G. (1996). *rbohA*, a rice homologue of the mammalian *gp91phox* respiratory burst oxidase gene. Plant J. *10*, 515–522.

Gumienny, T.L., Lambie, E., Hartwieg, E., Horvitz, H.R., and Hengartner, M.O. (1999). Genetic control of cell death in the *Caenorhabditis elegans* hermaphrodite germline. Development *126*, 1011-1022.

Horton, R.M., Hunt, H.D., Ho, S.N., Pullen, J.K., and Pease, L.R. (1989). Engineering hybrid genes without the use of restriction enzymes: gene splicing by overlap extension. Gene *77*, 61–68.

Hückelhoven, R., Fodor, J., Preis, C., and Kogel, K.H. (1999). Hypersensitive cell death and papilla formation in barley attacked by the powdery mildew fungus are associated with H_2O_2 but not salicylic acid accumulation. Plant Physiol. *119*, 1251–1260.

Jones, D.A., and Jones, J.D.G. (1997). The role of leucine-rich repeat proteins in plant defenses. Adv. Bot. Res. *24*, 90–166.

Jørgensen, J.H. (1988). Genetic analysis of barley mutants with modifications of powdery mildew resistance gene *Ml-a12*. Genome *30*, 129–132.

Jørgensen, J.H. (1996). Effect of three suppressors on the expression of powdery mildew resistance in barley. Genome *39*, 492–498.

Kim, J.S., and Raines, R.T. (1994). Peptide tags for a dual affinity fusion system. Anal. Biochem. *219*, 165–166.

Kitagawa, K., Skowyra, D., Elledge, S.J., Harper, J.W., and Hieter, P. (1999). Sgt1 encodes an essential component of the yeast kinetochore assembly pathway and a novel subunit of the SCF ubiquitin ligase complex. Mol. Cell *4*, 21–33.

Lahaye, T., Shirasu, K., and Schulze-Lefert, P. (1998). Chromosome landing at the barley *Rar1* locus. Mol. Gen. Genet. *260*, 92–101.

Lamb, C., and Dixon, R.A. (1997). The oxidative burst in plant disease resistance. Annu. Rev. Plant Physiol. Plant Mol. Biol. *48*, 251–275.

Levine, A., Tenhaken, R., Dixon, R., and Lamb, C. (1994). H_2O_2 from the oxidative burst orchestrates the plant hypersensitive disease resistance response. Cell *79*, 583–593.

Martin, W., Gierl, A., and Saedler, H. (1989). Molecular evidence for pre-cretaceous angiosperm origins. Nature *339*, 46–48.

Marcotte, E.M., Pellegrini, M., Ng, H.-L., Rice, D.W., Yeates, T.O.,

and Eisenberg, D. (1999). Detecting protein function and protein-protein interactions from genome sequences. Science *285*, 751–753.

Parniske, M., Hammond-Kosack, K.E., Golstein, C., Thomas, C.M., Jones, D.A., Harrison, K., Wulff, B.B.H., and Jones, J.D.G. (1997). Novel disease resistance specificities result from sequence exchange between tandemly repeated genes at the *Cf-4/9* locus of tomato. Cell *91*, 821–832.

Pennell, R.I., and Lamb, C. (1997). Programmed cell death in plants. Plant Cell *9*, 1157–1168.

Peterhänsel, C., Freialdenhoven, A., Kurth, J., Kolsch, R., and Schulze-Lefert, P. (1997). Interaction analyses of genes required for resistance responses to powdery mildew in barley reveal distinct pathways leading to leaf cell death. Plant Cell *9*, 1397–1409.

Sanchez-Garcia, I., and Rabbitts, T.H. (1994). The LIM domain: a new structural motif found in zinc-finger-like Proteins. Trends Genet. *10*, 315–320.

Schiffer, R., Görg, R., Jarosch, B., Beckhove, U., Bahrenberg, G., Kogel, K.-H., and Schulze-Lefert, P. (1997). Tissue dependence and differential cordycepin sensitivity of race-specific resistance responses in the barley-powdery mildew interaction. Mol. Plant-Microbe Interact. *10*, 830–839.

Schwabe, J.W.R., and Klug, A. (1994). Zinc mining for protein domains. Nat. Struct. Biol. *1*, 345–349.

Shirasu, K., Nakajima, H., Rajasekhar, V.K., Dixon, R.A., and Lamb, C. (1997). Salicylic acid potentiates an agonist-dependent gain control that amplifies pathogen signal in the activation of defense mechanisms. Plant Cell *9*, 261–270.

Thordal-Christensen, H., Zhang, Z., Wei, Y., and Collinge, D.B. (1997). Subcellular localization of H_2O_2 in plants. H_2O_2 accumulation in papillae and hypersensitive response during the barley-powdery mildew interaction. Plant J. *11*, 1187–1194.

Torp, J., and Jørgensen, J.H. (1986). Modification of barley powdery mildew resistance gene *Ml-a12* by induced mutation. Can. J. Genet. Cytol. *28*, 725–731.

Van der Biezen, E.A., and Jones, J.D.G. (1998). The NB-ARC domain: a novel signaling motif shared by plant resistance gene products and regulators of cell death in animals. Curr. Biol. *8*, R226–R227.

Vaux, D.L., and Korsmeyer, S.J. (1999). Cell death in development. Cell *96*, 245–254.

Von Röpenack, E., Parr, A., and Schulze-Lefert, P. (1998). Structural analysis and dynamics of soluble and cell wall-bound phenolics in a broad spectrum resistance to the powdery mildew fungus in barley. J. Biol. Chem. *273*, 9013–9022.

Webster, L.C., Zhang, K., Chance, B., Ayene, I., Culp, J.S., Huang, W.J., Wu, F.Y.H., and Ricaciardi, R.P. (1991). Conversion of the E1A Cys4 zinc finger to a nonfunctional His2, Cys2 zinc finger by a single point mutation. Proc. Natl. Acad. Sci. USA *88*, 9989–9993.

Wei, F., Gobelman-Werner, K., Morroll, S.M., Kurth, J., Mao, L., Wing, R., Leister, D., Schulze-Lefert, P., and Wise, R.P. (1999). The *Mla* (powdery mildew) resistance cluster is associated with three NBS-LRR gene families and suppressed recombination within a 300-kb DNA interval on chromosome 5S (1Hs) of barley. Genetics, in press.

GenBank Accession Numbers

Barley *Rar1* (AF192261), *Arabidopsis Rar1* (AF192262), *Toxoplasma Rar1* (AF192263), *C. elegans chp* (AF192264), *Drosophila Chp* (AF192465), human *CHP1* (AF192466), and rice *Sgt1* (AF192467) sequences have been deposited into the GenBank database.